Mesospheric inversions and their relationship to planetary wave structure

Murry Salby,[1] Fabrizio Sassi,[2] Patrick Callaghan,[2] Dong Wu,[3] Philippe Keckhut,[4] and Alain Hauchecorne[4]

Received 23 April 2001; revised 7 September 2001; accepted 12 September 2001; published 28 February 2002.

[1] Mesospheric inversions are studied in vertical soundings from the French lidar at Observatoire de Haute-Provence and in synoptic global structure that was observed simultaneously by the UARS satellite. The latter provides the instantaneous three-dimensional (3-D) structure of the circulation that accompanies mesospheric inversions. A numerical simulation with a 3-D primitive equation model is then shown to reproduce major features of the observed behavior. Both reveal an extensive pattern of inverted thermal structure. The behavior is closely related to planetary waves, which, in the model, experience strong absorption in the upper mesosphere and lower thermosphere. Inverted thermal structure mirrors the synoptic pattern of potential vorticity, which marks the polar night vortex. Both are strongly distorted during stratospheric warmings, when inverted thermal structure at midlatitudes is favored. The region of negative lapse rate coincides with those altitudes where planetary wave temperature undergoes an abrupt phase shift. Wave temperature is then driven out of phase with wave geopotential. This alters the vertical structure of planetary waves, from westward tilt and upward amplification below the inversion to nearly barotropic structure and upward decay above the inversion. Accompanying the upward decay of planetary waves above the inversion is a decay of flow distortion, as the disturbed vortex is gradually restored toward polar symmetry. *INDEX TERMS:* 3332 Meteorology and Atmospheric Dynamics: Mesospheric dynamics; 3334 Meteorology and Atmospheric Dynamics: Middle atmosphere dynamics (0341, 0342); 3384 Meteorology and Atmospheric Dynamics: Waves and tides; *KEYWORDS:* Inversion, mesosphere, planetary waves

1. Introduction

[2] Measurements of thermal structure reveal the sporadic occurrence of temperature inversions in the mesosphere, which is normally characterized by a positive lapse of temperature [*Schmidlin*, 1976; *Hauchecorne et al.*, 1987]. After developing, these regions of negative lapse rate survive for several days [*Leblanc et al.*, 1995]. They form preferentially at altitudes of 65–75 km, at midlatitudes, and during the disturbed months of winter [*Leblanc and Hauchecorne*, 1997].

[3] Several explanations have been proposed for this anomalous thermal structure. Notable are mechanisms involving gravity waves and thermal tides [e.g., *Hauchecorne et al.*, 1987; *Liu et al.*, 2000]. However, anomalous thermal structure often persists for several days. It is also observed simultaneously at sites that are separated by several thousand kilometers. Recently, global measurements from the UARS satellite have shown that mesospheric inversions accompany large-scale perturbations that are associated with planetary waves [*Wu*, 2000].

[4] Here we investigate the relationship between mesospheric inversions and planetary waves in a two-pronged analysis: The three-dimensional (3-D) structure of mesospheric inversions is studied first in vertical soundings from the French lidar at Observatoire de Haute-Provence (OHP) and in simultaneous observations of synoptic global structure observed by UARS. Their structure is then simulated in nonlinear integrations with a 3-D primitive equation model.

[5] Following a review of the data and model, section 3 dissects the observed vertical and horizontal structure of mesospheric inversions. Section 4 interprets the 3-D structure in terms of planetary waves, which are observed simultaneously. A numerical simulation is then performed in section 5, under conditions representative of those under which mesospheric inversions are observed. It is shown to reproduce major features of the observed thermal structure. Observed and simulated structures are both consistent with the behavior expected from planetary waves, which experience strong absorption in the upper mesosphere and lower thermosphere.

2. Observational and Numerical Frameworks

2.1. Data

[6] The Rayleigh lidar at OHP (6°E, 44°N) observes thermal structure above 30 km with high vertical resolution and little dependence on calibration and instrumental changes. Temperature is deduced from Rayleigh scattering [*Hauchecorne and Chanin*, 1980]. This technique recovers thermal structure through the mesosphere, with good signal-to-noise between 30 and 80 km. Routine monitoring has produced a record of temperature structure over OHP dating back to 1979.

[7] During the operational phase of UARS (September 1991–August 1993), temperature structure was simultaneously observed from space. The Improved Stratospheric and Mesospheric Sounder (ISAMS) provided temperature retrievals up to 70 km, higher altitudes relying increasingly on climatology. However, ISAMS operated for only 6 months before suffering a mechanical failure. The Microwave Limb Sounder (MLS), also on board UARS,

[1]Program in Atmospheric and Oceanic Sciences, University of Colorado, Boulder, Colorado, USA.
[2]Atmospheric Systems and Analysis, Westminster, Colorado, USA.
[3]Jet Propulsion Laboratory, California Institute of Technology, Pasadena, California, USA.
[4]Service d'Aeronomie, Centre National de la Recherche Scientifique, Verrieres-le-Buisson, France.

0148-0227/02/2001JD000756$09.00

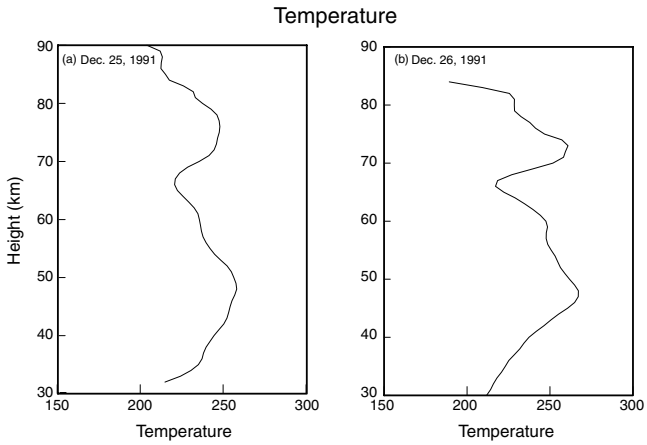

Figure 1. Temperature profile observed over OHP on (a) 25 December 1991 and (b) 26 December 1991.

measured temperature in the stratosphere and mesosphere as well. Prior to Version 5, temperature was retrieved from MLS only at 46–4.6 hPa, falling short of the region of mesospheric inversions. The Version 5 retrieval extends to ~85 km. However, vertical resolution at those altitudes is poor, unable to resolve any mesosphere inversions.

[8] Recently, an advanced algorithm, which uses all 63-GHz radiances and accounts for the geomagnetic Zeeman effect, is able to recover temperature up to 90 km [*Wu*, 2000; D. Wu et al., Retrieval and validation of MLS 63-GHz mesospheric temperature, submitted to *Journal of Atmospheric and Solar-Terrestrial Physics*, 2001]. This retrieval has vertical resolution of ~10 km and precision better than 8 K below 85 km, where mesospheric inversions form. It expands MLS measurements up to and beyond the altitudes recovered by ISAMS. Moreover, the temperature record produced then extends over the longer operational phase of MLS, which continued to function over the rest of the decade.

[9] Measurements from both instruments are asynoptic: Different sites are observed at different times. They have been used to map thermal structure synoptically [*Sassi and Salby*, 1998], in which temperature is available simultaneously over the entire globe; for a review of this topic, see *Salby* [1989] and references therein. The operational mapping algorithm makes use of the information and error characteristics of instruments observing a field property. Twice-daily synoptic maps provide 3-D thermal structure that is nearly simultaneous with the vertical soundings of temperature from the OHP lidar. From these, geopotential, motion, and quasi-geostrophic potential vorticity are constructed above 30 mbar, where structure is prescribed from the European Centre for Medium-Range Weather Forecasts analyses; a description of these standard meteorological quantities can be found in texts by *Holton* [1992] and *Salby* [1996]. The analysis below uses these joint measurements to piece together the instantaneous 3-D structure of the circulation that accompanies mesospheric inversions.

2.2. Three-Dimensional Model

[10] Thermal structure is simulated with a nonlinear primitive equation model [*Callaghan et al.*, 1999]. The model, which is spectral in all three directions, solves the governing equations in isentropic coordinates; a review of isentropic coordinates can be found in the above texts. It extends from a level near the tropopause, where integrations are forced by planetary wave structure, through the mesosphere. Higher altitudes comprise a deep sponge layer, which enforces the radiation condition by absorbing upward propagating wave activity.

[11] Integrations forced by observed wave structure reproduce major features of the wintertime circulation of the middle atmosphere. Included are zonal mean dynamical structure, climatological features associated with planetary waves, and mean diabatic motion [ibid; *Fusco and Salby*, 1999a, 1999b; *Francis and Salby*, 2001]. The resemblance of these features to observed behavior provides a framework in which mesospheric inversions can be studied.

3. Observed Thermal Structure

[12] Figure 1 shows temperature soundings over OHP on 25 and 26 December 1991. On 25 December (Figure 1a) the positive lapse of temperature that normally prevails above 45 km is interrupted above 65 km. Thermal structure is inverted between 66 and 72 km, where temperature increases from ~220 K to 245 K. It corresponds to a negative lapse rate of about -5 K/km. This inversion is capped overhead by an isothermal layer, ~5 km deep. At higher levels, the positive lapse of temperature is restored. A day later (Figure 1b), the inversion is still visible but has shallowed and steepened: Temperature now increases between 67 and 71 km, from ~220 K to 260 K. There, it corresponds to a negative lapse rate exceeding -10 K/km.

[13] Analogous structure is shown in Figure 2 for 3 and 4 January 1993. On 3 January (Figure 2a) a temperature inversion has formed between 67 and 72 km. It corresponds to a negative lapse rate of about -5 K/km. The inverted thermal structure is capped overhead by a deep nearly isothermal layer that extends upward to 90 km. A day later (Figure 2b), the inversion is still visible and has steepened somewhat. Also appearing then is a second inversion, found above 80 km, before the positive lapse of temperature is restored at higher altitudes.

[14] Inversions observed over OHP are actually part of anomalous thermal structure that is more extensive. Figure 3 plots, as a cross section of longitude and altitude, the synoptic structure of temperature at 44°N (contoured) observed by UARS on 25 December 1991. Regions of negative lapse rate are shaded. Temperature is inverted below 45 km, in the stratosphere. Notice that inverted thermal structure there varies with longitude, like temperature. At those levels, negative lapse rate is highest and strongest in the Eastern Hemisphere, coincident with the cold anomaly of the planetary wave field (where isotherms are deflected upward). (Note, the term "anomaly" refers to the departure from the zonal mean.) Conversely, negative lapse rate is lowest and weakest just east of the dateline, coincident with the warm anomaly of the planetary wave field (where isotherms are deflected downward).

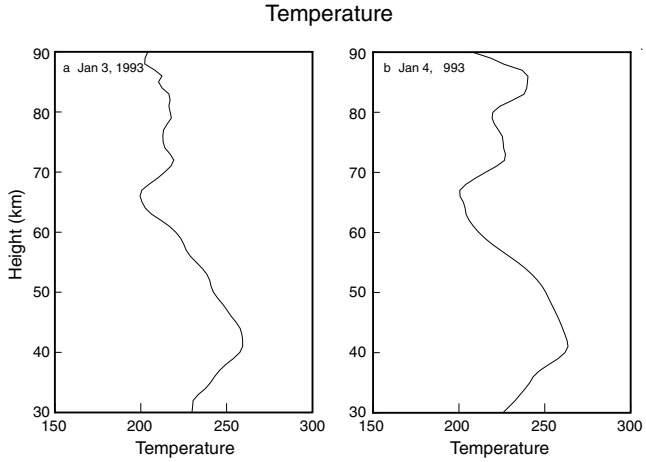

Figure 2. As in Figure 1, but on (a) 3 January 1993 and (b) 4 January 1993.

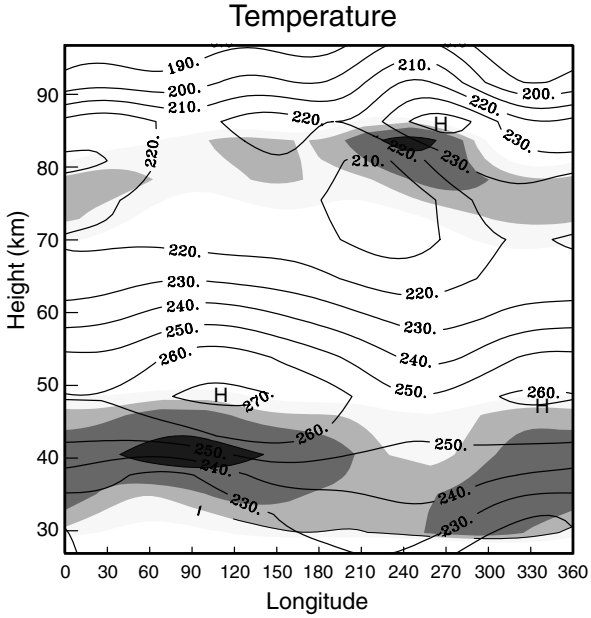

Figure 3. Temperature (Kelvin) at 44°N, as a cross section of longitude and height, observed by UARS on 25 December 1991. Superposed are regions of negative lapse rate (shaded).

[15] Thermal structure is also inverted above 65 km, in the mesosphere. The positive lapse of temperature characteristic of these altitudes is interrupted by a nearly isothermal layer that is some 15 km deep. It is most noticeable between 90°E and 270°E, but the lapse of temperature is interrupted around much of the globe. Along the upper boundary of the isothermal layer is the mesospheric inversion that was observed contemporaneously at OHP (Figure 1a). (At the longitude of OHP the layer of negative lapse rate extends somewhat higher than the inversion observed by the lidar. The minor difference reflects the somewhat coarser vertical resolution of the satellite retrieval.) The inversion observed at OHP thus represents a vertical section of a more extensive anomaly that spans much of the Earth. A day later (not shown) the inverted thermal structure is still visible across much of the globe, as it is in the vertical profile over OHP (Figure 1b).

[16] Like inverted thermal structure in the stratosphere, the mesospheric inversion in Figure 3 varies with longitude. It is highest and strongest in the Western Hemisphere, immediately above the cold wave anomaly in the lower mesosphere near 225°E (where isotherms are deflected downward). The cold anomaly reaches a maximum near 72 km, capped overhead by a warm anomaly. Together, these oppositely signed features produce the strong inversion found at these longitudes. The cold anomaly's replacement by a warm anomaly overhead and to its east represents an abrupt phase shift of wave temperature T'. It swings T' in the upper mesosphere a quarter cycle out of phase with T' at lower levels. Coinciding with this phase shift is the layer of inverted thermal structure.

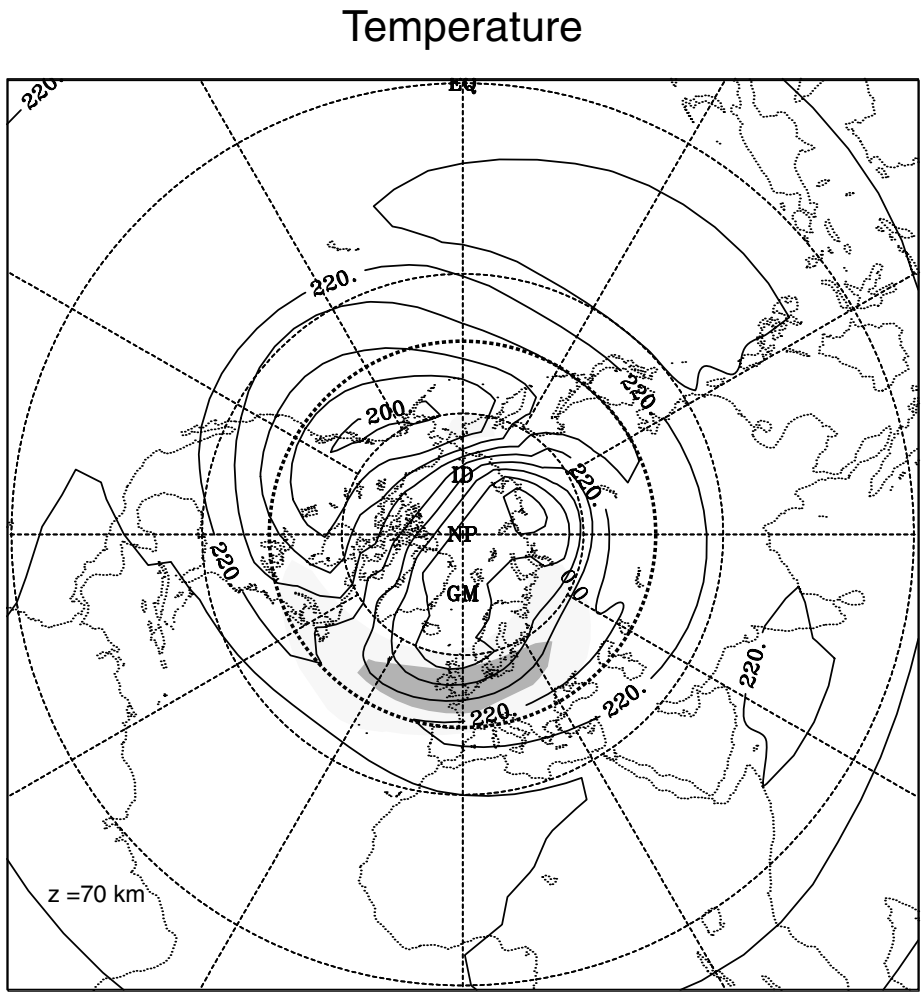

Figure 4. Synoptic map of temperature at 70 km observed by UARS on 25 December 1991. Superposed are regions of negative lapse rate (shaded) and latitude of OHP (dashed).

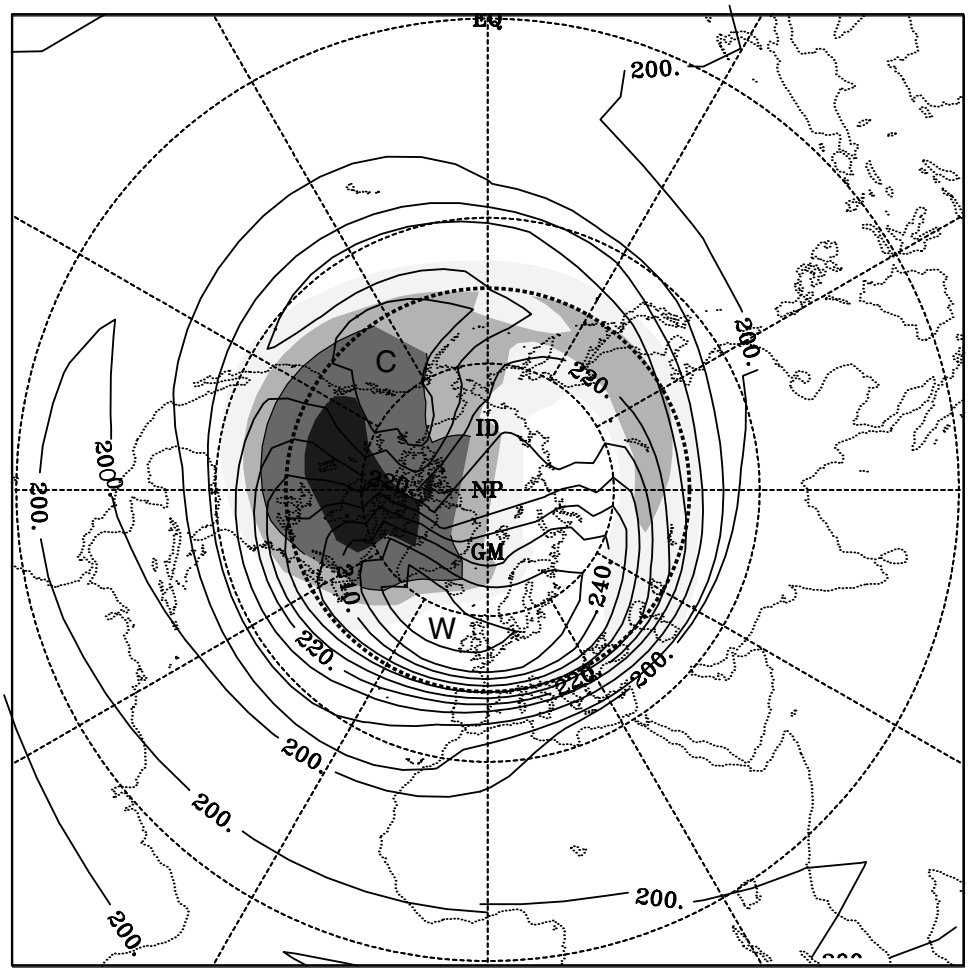

Figure 5. As in Figure 4, but at 81 km.

[17] Elsewhere, the mesospheric inversion is lowest just east of Greenwich. There, too, a cold wave anomaly in the lower mesosphere (isotherms deflected downward) is capped overhead by a warm anomaly (isotherms deflected upward), which maximizes near 80 km. As in the Western Hemisphere, this represents a reversal of wave temperature and an abrupt phase shift of T'. Coinciding with it is the layer of inverted thermal structure.

[18] Vertical structure in Figure 3 corresponds to horizontal thermal structure that likewise follows the planetary wave field. Figure 4 shows the contemporaneous synoptic map of temperature at 70 km. This level slices through the base of the inversion near Greenwich (shaded), where it coincides with the warm wave anomaly. Inverted thermal structure at 70 km is seen to extend from North America, across the Atlantic, and into Eurasia. Opposite the pole, temperature is dominated by the cold wave anomaly, which lies beneath the mesospheric inversion. The cold anomaly that prevails there places inverted thermal structure and the warm anomaly overlying it at higher altitude.

[19] Figure 5 presents the synoptic map of temperature at 81 km, a level that slices through the top of the inversion and the steepest negative lapse rate. The warm anomaly is intensified at this altitude, reflecting inverted thermal structure below. Negative lapse rate at 81 km (shaded) is now positioned between the warm and cold anomalies. Each has shifted abruptly towards the west (cf. Figure 4), albeit less so for the cold anomaly. At altitudes above the inversion (not shown), the warm anomaly is shifted farther west. It is then centered near 60°W, which places T' there a quarter cycle out of phase with T' beneath the inversion.

4. Relationship to Planetary Wave Structure

[20] The abrupt shift of temperature phase found at levels of the inversion reflects a change in the character of planetary waves. Anomalous thermal structure in Figures 3–5 is related to isobaric geopotential Φ. Proportional to stream function, Φ directly characterizes the planetary wave field [see, e.g., *Holton*, 1992; *Salby*, 1996]. From hydrostatic balance in log pressure coordinates,

$$\begin{aligned} \tfrac{\partial \Phi}{\partial z} &= \tfrac{RT}{H} \\ H &= \tfrac{RT_0}{g}, \end{aligned} \tag{1}$$

temperature determines the rate at which geopotential increases upward. The lapse rate

$$\Gamma = -\frac{\partial T}{\partial z} \tag{2}$$

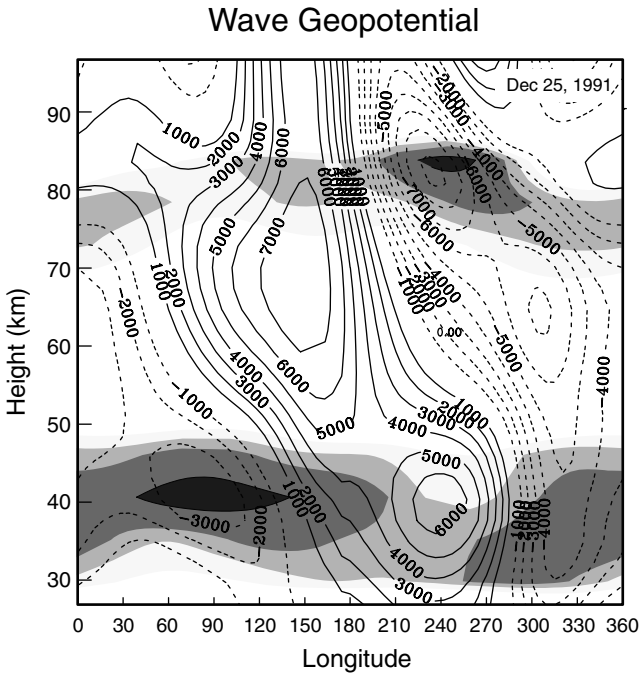

Figure 6. Wave geopotential ($m^2\ s^{-2}$) at 44°N, as a cross section of longitude and height, observed by UARS on 25 December 1991.

is then related to geopotential through its vertical curvature

$$\Gamma = -\frac{H}{R}\frac{\partial^2 \Phi}{\partial z^2}. \tag{3}$$

Separating field properties into zonal mean and wave components,

$$\Gamma = \bar{\Gamma} + \Gamma', \tag{4}$$

shows that thermal structure can be inverted ($\Gamma < 0$) in the mesosphere, where $\bar{\Gamma} > 0$, if

$$\begin{aligned} \Gamma' &= -\tfrac{H}{R}\tfrac{\partial^2 \Phi'}{\partial z^2} \\ &< -\bar{\Gamma}, \end{aligned} \tag{5}$$

i.e., if Γ' is sufficiently negative or, equivalently, if the vertical curvature of Φ' is sufficiently positive. This condition is favored in regions where wave temperature T' changes sharply, which translates into an abrupt change of wave structure Φ'.

[21] Figure 6 shows, as a cross section of longitude and altitude, the wave geopotential on 25 December 1991. Through the stratosphere and lower mesosphere, Φ' slopes westward with altitude, corresponding to upward propagation of planetary wave activity. It amplifies with altitude, also consistent with upward propagation, until reaching a maximum in the upper mesosphere. Above the maximum, westward tilt weakens or disappears altogether. Planetary wave structure then becomes barotropic, with phase contours nearly vertical (i.e., no upward variation of phase). The change of wave structure is most noticeable between 90°E and 270°E, where wave geopotential is large. This is the same range of longitude where temperature becomes nearly isothermal (Figure 3) and then shifts out of phase at higher levels.

[22] The mesospheric inversion (shaded) is found at and just above the level of maximum wave amplitude. It caps the region of westward tilt at lower levels. Above the inversion, vertical phase tilt weakens or disappears altogether, replaced by nearly barotropic structure in which wave activity decays. The change of structure in Figure 6 corresponds to strong absorption of planetary waves, for example, by turbulent mixing associated with gravity wave breaking and by thermal dissipation associated with nonlocal thermodynamic equilibrium. Both prevail in the upper mesosphere and lower thermosphere.

[23] The mesospheric inversion is steepest in and slightly above the negative maximum of wave geopotential, where Φ' is large and negative. There, sharp decay overhead makes the vertical curvature of Φ' strong and positive (5). Notice that negative Φ' still slopes westward above the inversion, but much less than beneath the inversion. The region of strong vertical curvature also lies just above where the cold wave anomaly at lower levels reaches a maximum (Figure 3), abruptly shifting phase at higher levels to become a warm anomaly. At other longitudes, the inversion is weaker. However, even there, it tends to follow the level of maximum vertical curvature of Φ', which divides westward tilt and upward amplification below from nearly barotropic structure and decay overhead. The inversion is positioned just above the positive maximum of Φ'. This is where planetary wave structure becomes external: wave energy decaying upward, with little or no phase tilt. Φ' then assumes positive curvature, as wave activity density decays overhead. At intermediate longitudes, the inversion is some 5 km lower. It coincides with a transition from negative to positive Φ' in which vertical curvature again maximizes.

[24] The change in wave structure at levels of the inversion coincides with the abrupt phase shift of wave temperature (Figure 3). Below 72 km a cold anomaly is positioned in the Western Hemisphere. It is nearly in quadrature with the geopotential anomaly (Figure 6). By (1), Φ' then varies with altitude as e^{ikz}. It thus slopes westward and amplifies upward through the stratosphere and lower mesosphere. The cold anomaly reaches a maximum near 225°E and 72 km. It is replaced overhead by a strong warm anomaly, which eventually becomes out of phase with the cold anomaly at lower levels. The abrupt phase shift of wave temperature positions T' out of phase with Φ' above the inversion. From (1), Φ' then varies with altitude as e^{-kz}. Consequently, wave geopotential (more precisely, wave activity density, e.g., $\rho|\Phi'|^2$) decays at higher altitudes, where

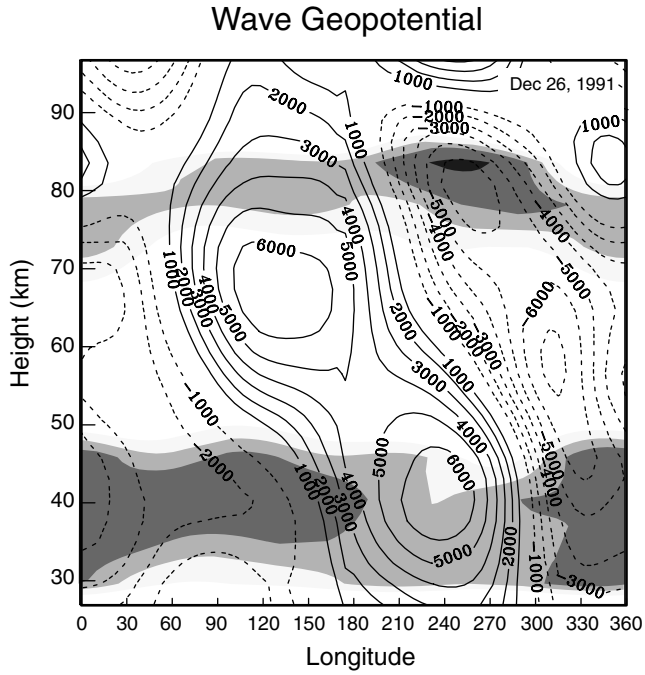

Figure 7. As in Figure 6, but on 26 December 1991.

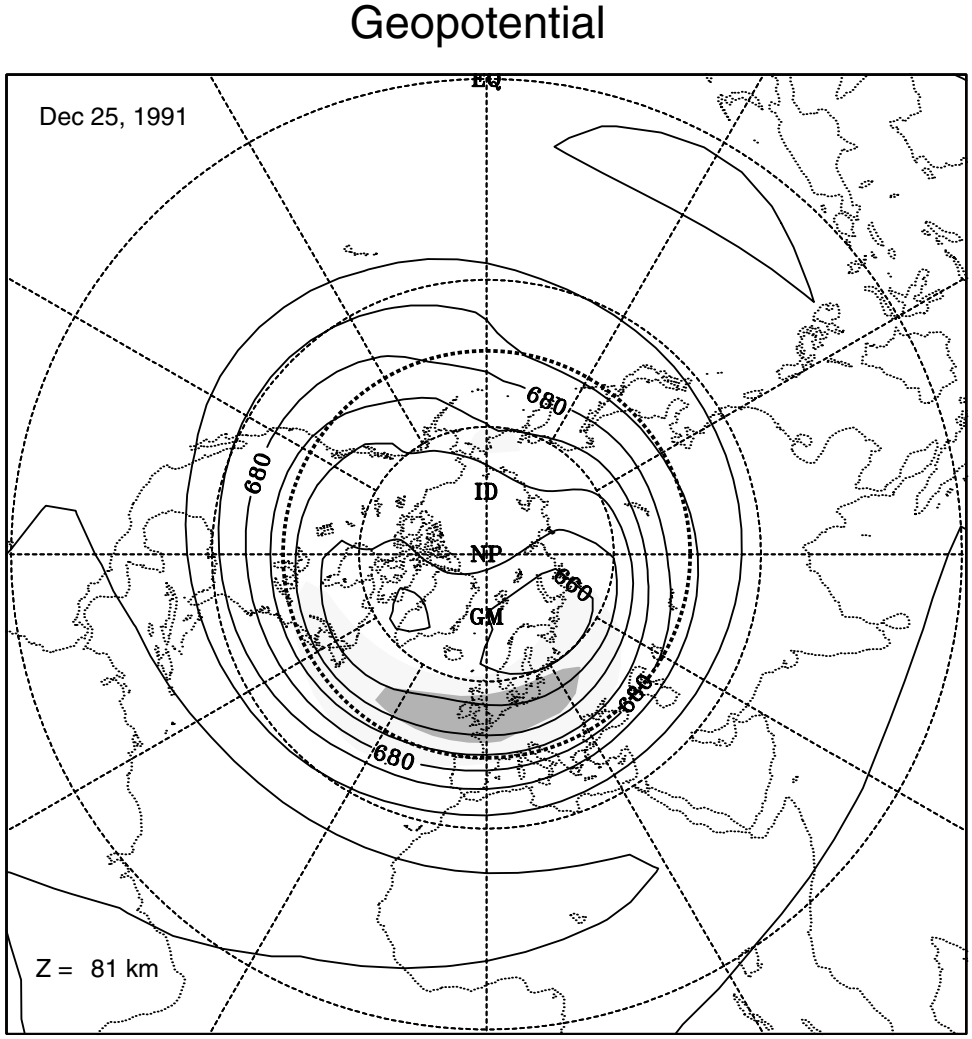

Figure 8. Synoptic map of geopotential (m^2/s^2) at 70 km on 25 December 1991, scaled by 1000, derived from UARS observations. Superposed are regions of negative lapse rate (shaded).

strong dissipation renders planetary waves external. The warm anomaly above 72 km, which accompanies inverted thermal structure, is thus introduced to cancel wave geopotential in the region of strong absorption. It continues upward through the roof of the UARS observations, the amplitude of Φ' decaying accordingly.

[25] The relationship between inverted thermal structure and the decay of planetary waves is even more conspicuous on the following day (Figure 7). This is when the inversion observed by the OHP lidar is intensified (Figure 1b). Positive and negative height anomalies then both decay sharply above the inversion, where they exhibit little or no phase tilt. This contrasts with the continuous westward tilt and upward amplification observed beneath the inversion. The layer of inverted thermal structure again lies at or just above the level of maximum wave amplitude. As on the preceding day, it coincides with strong positive curvature of Φ', where wave geopotential satisfies (5). Higher, wave geopotential decays and becomes barotropic. External structure, visible now at all longitudes above the inversion, implies that planetary waves have, by this time, suffered strong absorption.

[26] The relationship to horizontal wave structure, seen earlier in temperature, is even clearer in geopotential. Figure 8 shows, for December 25, 1991, the synoptic map of Φ at 70 km. The wave field is amplified at middle and high latitudes. Minimum geopotential at high latitudes stretches eastward from North America into Eurasia, forming a crescent pattern. It reflects the polar night vortex being displaced equatorward toward Greenwich, corresponding to the negative anomaly of Φ' in Figure 6. Opposite the pole, the minimum is flanked by maximum geopotential near 150°E that invades the polar cap. It reflects the Aleutian high, corresponding to the positive anomaly of Φ' in Figure 6.

[27] Mirroring the crescent pattern of wave geopotential is the region of inverted thermal structure at 70 km. Negative lapse rate extends continuously from Canada, across the Atlantic, and into Eurasia. Its structure resembles the much noisier pattern of individual UARS soundings collected on this day [*Leblanc et al.*, 1995]. The synoptic structure in Figure 8, on the other hand, describes changes that operate coherently (and are therefore resolved in the asynoptic measurements). It reveals a continuous anomaly of negative lapse rate that extends from 90°W to 90°E. On the day shown, OHP lies at the southern edge of the steepest inversion. A day later (not shown), that feature expands eastward, along with planetary wave structure.

[28] The structure of wave geopotential in Figure 8 is nearly in quadrature with wave temperature at 70 km (Figure 4): T' possesses a node near 30°W and 150°E, approximately the longitudes of minimum and maximum Φ'. By (1), Φ' then varies with

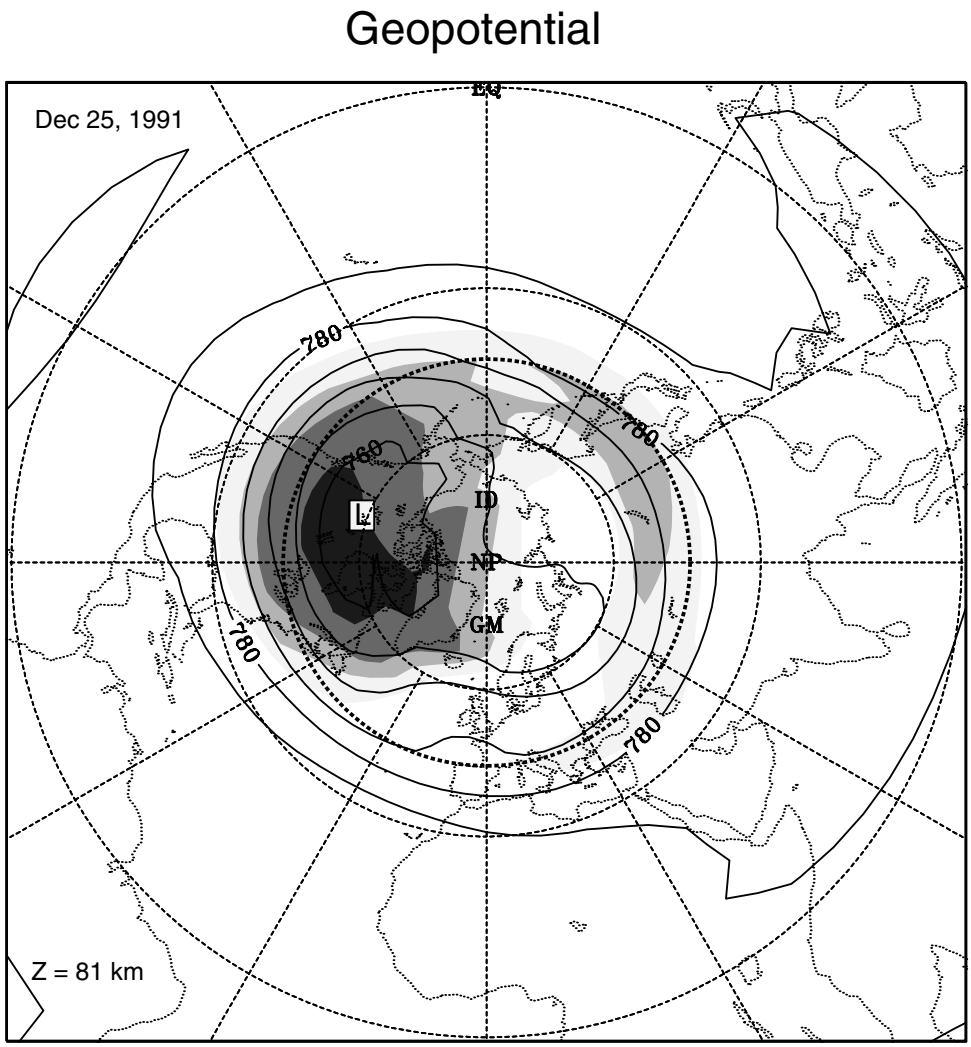

Figure 9. As in Figure 8, but at 81 km.

altitude as e^{ikz}. At this level, which lies mostly beneath the inversion, Φ' and T' thus represent upward propagation of planetary wave activity.

[29] Above the inversion, the relationship between geopotential and temperature changes. Figure 9 shows the synoptic map of Φ at 81 km, which slices through the top of the inversion and the region of steepest negative lapse rate. The structure of wave geopotential is now almost out of phase with wave temperature. The intensified warm anomaly in Figure 5 is positioned over low Φ, which extends from 30°E to the dateline. At higher altitudes (not shown), Φ' becomes perfectly out of phase with T'. From (1), Φ' then varies with altitude as e^{-kz}, reflecting a cancellation at higher levels. Wave geopotential then decays upward.

[30] As at lower levels, the region of inverted thermal structure in Figure 9 resembles the geopotential minimum, about which it is concentrated. Both have shifted westward and intensified. The deep minimum of Φ corresponds to the negative geopotential anomaly in Figure 6. After sloping westward and intensifying, negative Φ' reaches a maximum just beneath the inversion. It then decays overhead, with barotropic vertical structure.

[31] Even stronger is the relationship to potential vorticity (PV). Shown at 70 km in Figure 10, it has been calculated from the synoptically mapped UARS fields. On 25 December 1991 (Figure 10a), the vortex (marked by high PV) has been displaced off the pole toward Greenwich. It has been distorted into a crescent shape by the Aleutian high (marked by low PV), which invades the Arctic from opposite the pole. The exaggerated displacement of the vortex characterizes a wave number 1 stratospheric warming, wherein the vortex is displaced out of polar symmetry by an amplified ridge that invades the polar cap. In the warming pictured, high-PV air extends from 90°W to 90°E, nearly parallel to latitude circles. Mirroring it is the region of inverted thermal structure (shaded).

[32] On 26 December (Figure 10b) the head of the vortex (marked by the PV maximum) has advanced eastward some 60°, now positioned over Siberia. Simultaneously, its tail has been stretched further westward by the anticyclonic circulation (low PV), which now prevails over the polar cap. The tail of the vortex, positioned over western Canada, is seen to spiral poleward about a low-PV anomaly centered north of Hudson Bay. Despite the exaggerated distortion of the vortex, the region of inverted thermal structure remains virtually coincident with contours of high PV marking the vortex. In fact, contours of PV that break, as the rearward section of the vortex is strained westward, are mirrored by the region of inverted thermal structure. Both reappear as isolated

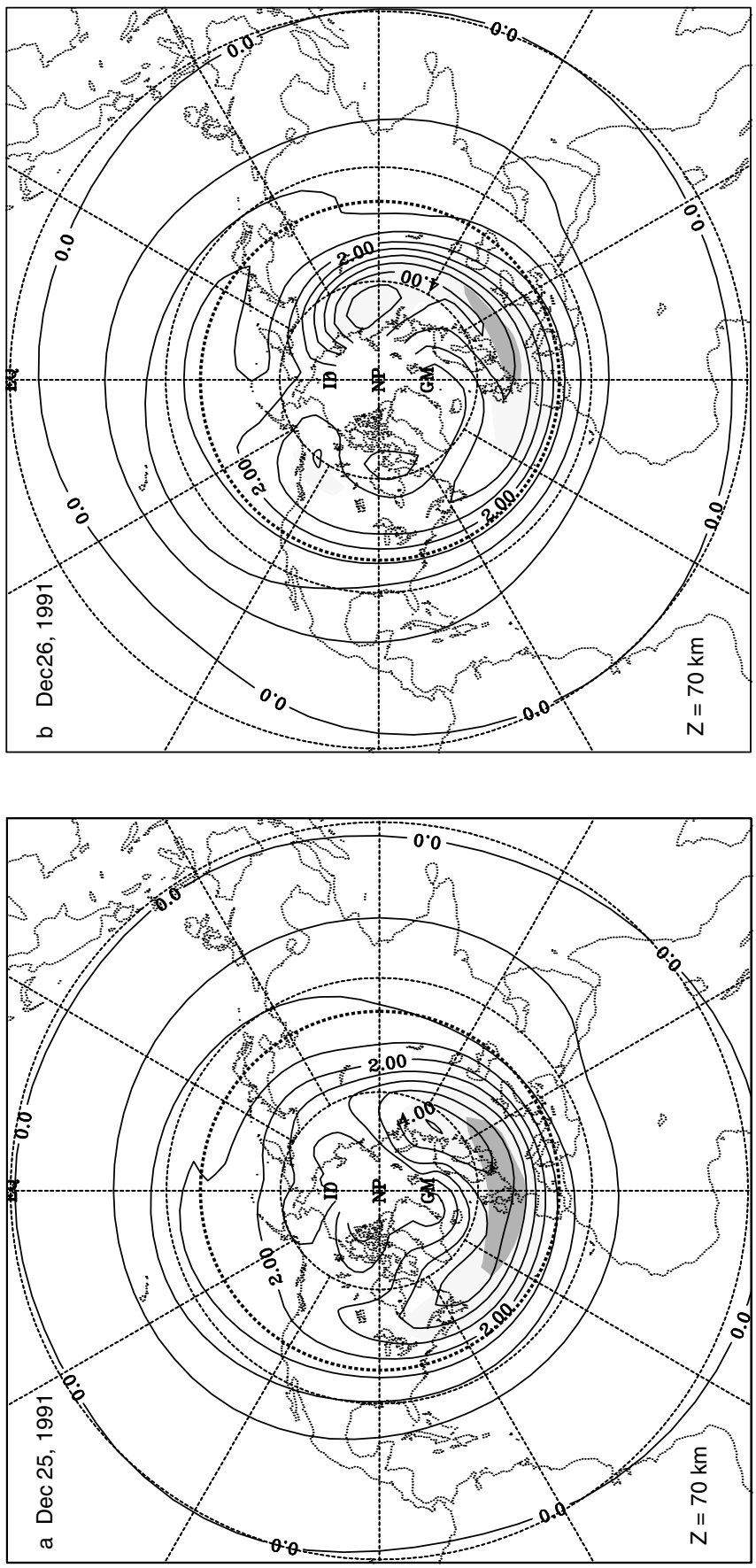

Figure 10. Synoptic map of potential vorticity at 70 km, derived from UARS observations, on (a) 25 December 1991 and (b) 26 December 1991. Superposed are regions of negative lapse rate (shaded).

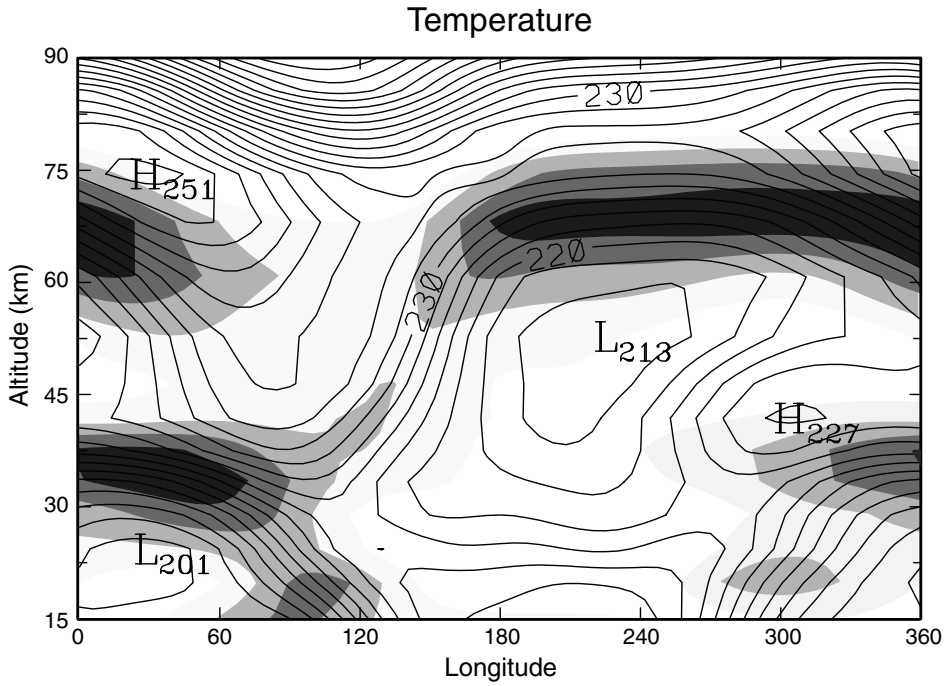

Figure 11. Temperature (Kelvin) at 65°N, as a cross section of longitude and height, during a wave number 1 stratospheric warming, as calculated in the 3-D primitive equation model. Superposed are regions of negative lapse rate (shaded).

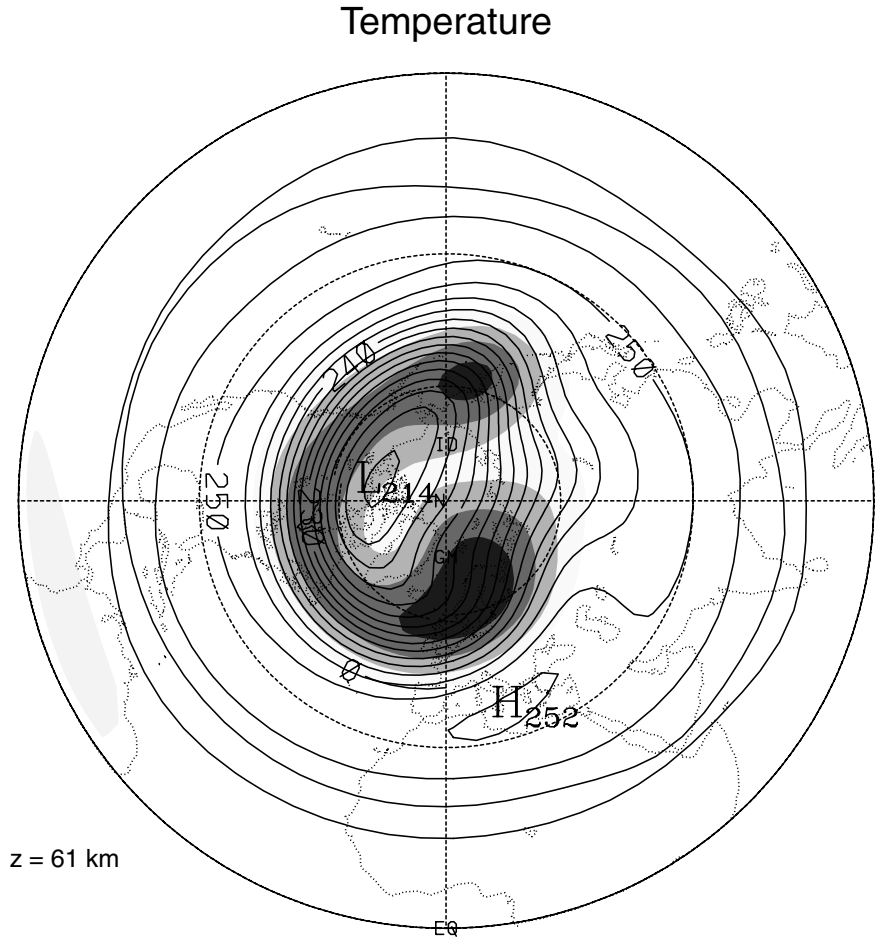

Figure 12. Horizontal map of temperature at 61 km during the calculated warming. Superposed are regions of negative lapse rate (shaded).

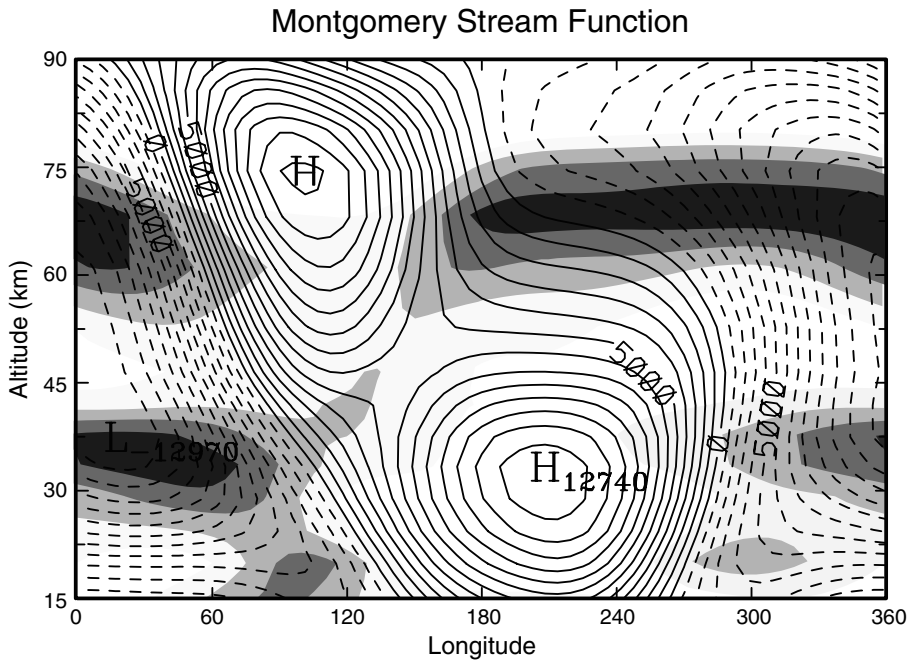

Figure 13. Wave Montgomery stream function (m^2s^{-2}) at 65°N, as a cross section of longitude and height, during the calculated warming.

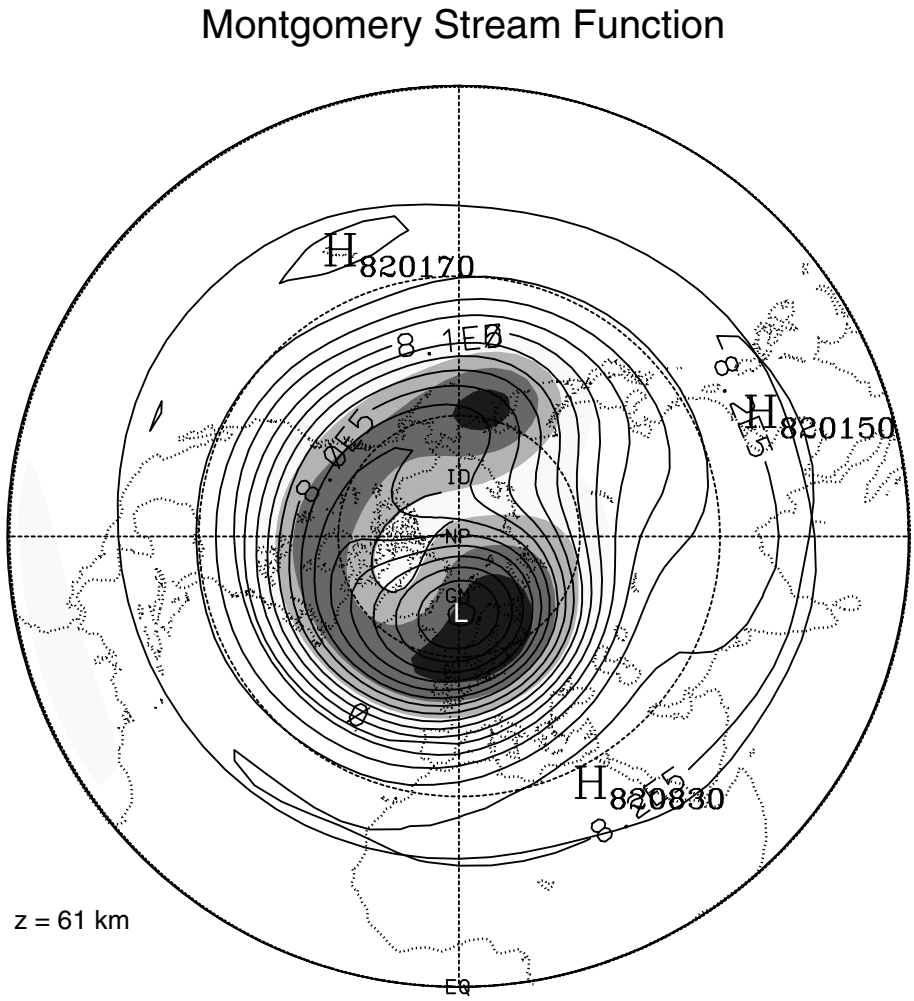

Figure 14. Horizontal map of Montgomery stream function at 61 km during the calculated warming.

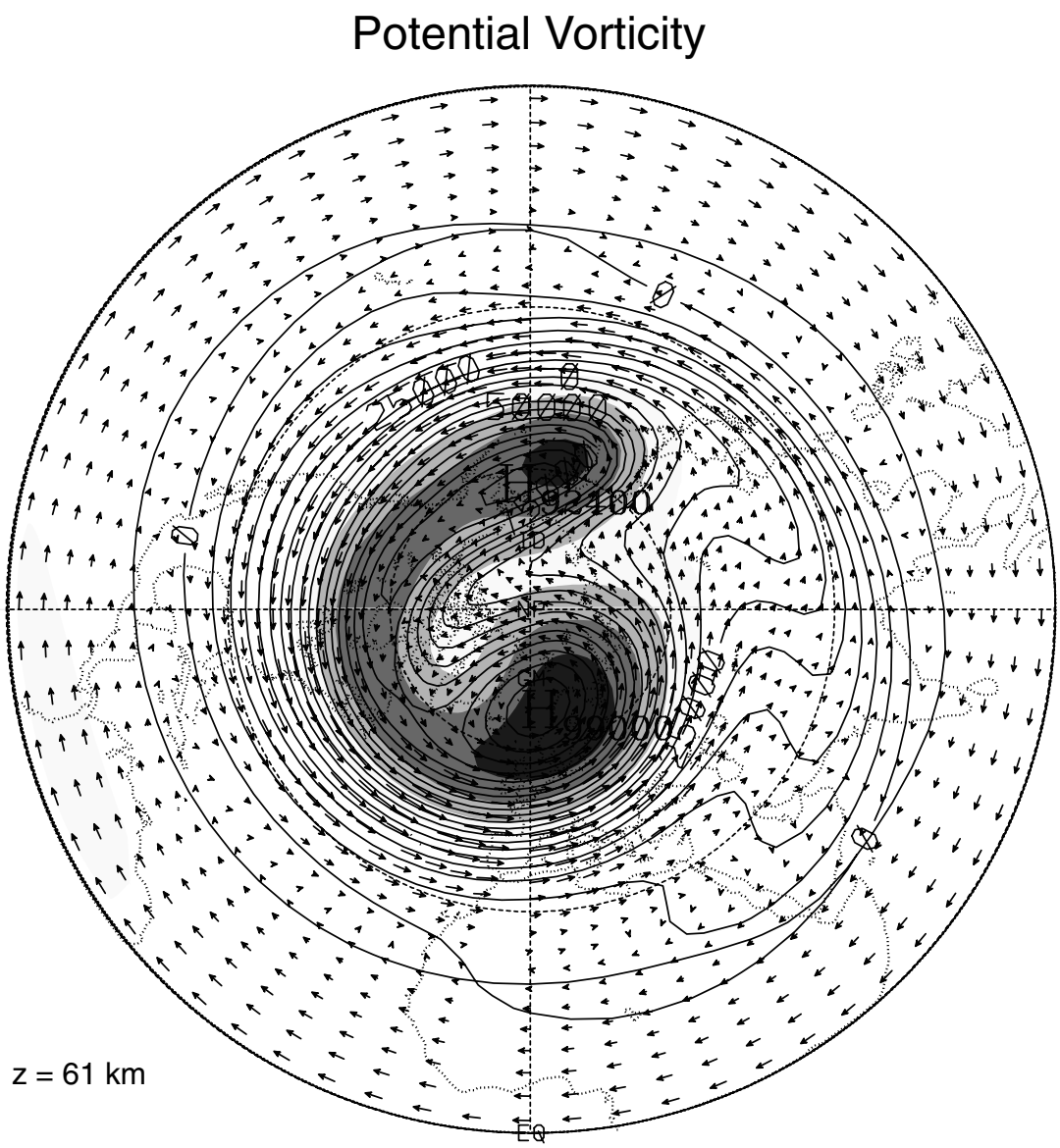

Figure 15. Horizontal map of potential vorticity at 61 km, along with the motion field, during the calculated warming. Superposed are regions of negative lapse rate (shaded).

anomalies in the tail of the vortex, which thereafter breaks away from the body of the vortex.

5. Simulated Thermal Structure

[33] Integrations have been performed with the 3-D model under perpetual January conditions, when inverted thermal structure in Figures 1–10 is observed. The model is forced by planetary wave structure near the tropopause representative of climatological mean conditions at this time of year [*Callaghan et al.*, 1999]. Through nonlinearity, integrations evolve transiently as planetary waves sporadically amplify, interact with the mean flow, and produce stratospheric warmings. Accompanying them are distortions of the polar night vortex, like that in Figure 10, which in turn are accompanied by mesospheric inversions.

[34] Figure 11 plots, as a cross section of longitude and altitude, the temperature at 65°N (contoured) during the mature phase of a wave number 1 warming. Inverted thermal structure (shaded), appears below 45 km in the stratosphere, where it is normally confined. In the Eastern Hemisphere, however, it protrudes above 45 km, the mean elevation of the stratopause. The region of negative lapse rate has, at this stage of the warming, actually folded over inverted thermal structure at lower levels in the stratosphere. Negative lapse rate in the mesosphere slopes westward and upward in the Eastern Hemisphere, crossing Greenwich and extending along the Western Hemisphere.

[35] Inverted thermal structure is highest in the Western Hemisphere, where it is positioned just above the cold anomaly near 225°E. There and westward across the dateline, isotherms are nearly vertical, analogous to the isothermal layer observed beneath the mesospheric inversion in Figure 3. The cold anomaly in Figure 11 reaches a maximum near 55 km, capped overhead by a warm anomaly that is centered a quarter cycle to its east. The warm anomaly slides into this position from the east and lower altitude, analogous to observed thermal structure in Figure 3. Separating the cold and warm anomalies is an abrupt shift in the phase of wave temperature. Collocated with this phase shift is the region of inverted thermal structure.

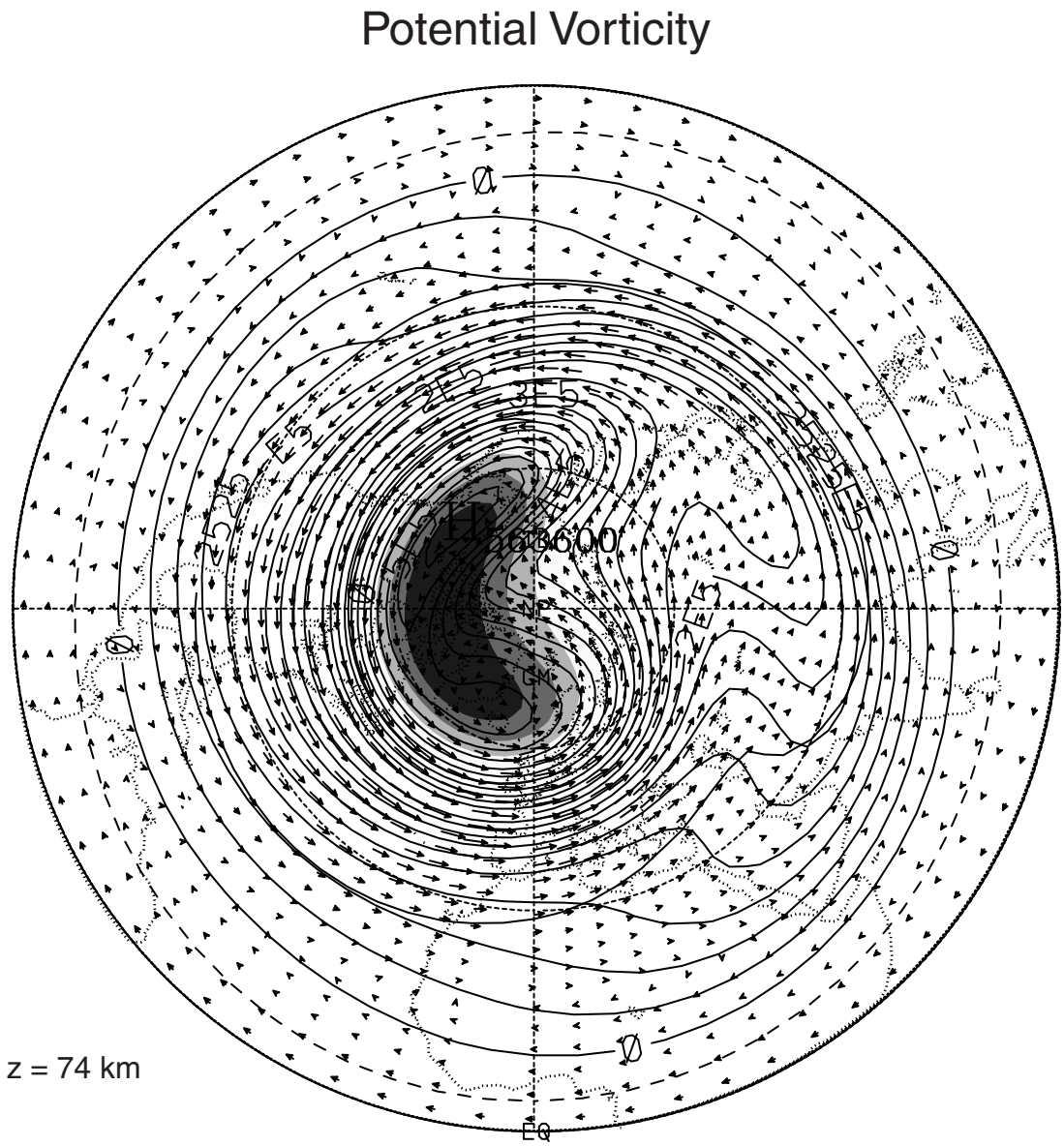

Figure 16. As in Figure 15, but at 74 km.

[36] Figure 12 shows, for the same time, the horizontal map of temperature at 61 km, which slices through the base of the inversion. Negative lapse rate (shaded) has been distorted into a crescent shape that extends westward from Greenwich, along the Western Hemisphere, and eventually crosses the dateline. Isotherms (contoured) are nearly in quadrature with this pattern: The cold anomaly is positioned near 90°W, centered over the distorted region of negative lapse rate. Flanking it opposite the pole is a warm anomaly.

[37] The abrupt phase shift of T' in Figure 11 is accompanied by a change in the vertical structure of planetary waves. Figure 13 plots the corresponding cross section of wave Montgomery stream function Ψ', which is the analogue in isentropic coordinates of wave geopotential Φ'. Negative Ψ' in the Eastern Hemisphere slopes westward and amplifies upward through the stratosphere, where it is nearly in quadrature with T' (Figure 11). At this stage of the warming, negative Ψ' reaches a maximum near Greenwich and 60 km. There, the abrupt shift of wave temperature drives T' out of phase with Ψ'. This brings to a halt vertical tilt and amplification, which are replaced overhead by nearly barotropic structure and vertical decay. Coinciding with the transition, where vertical curvature of Ψ' is positive and strong, is the mesospheric inversion.

[38] Analogous structure appears above the positive anomaly of Ψ'. On the day shown, positive Ψ' assumes barotropic structure with vertical decay near 225′E and above 30 km, before shifting westward and reamplifying above 45 km. It becomes truly external only above 85 km. The region near 225°E and above 30 km, where positive Ψ' becomes barotropic, overlies the cold anomaly (Figure 11). T' is then out of phase with Ψ'. Through hydrostatic balance in isentropic coordinates

$$\frac{\partial \Psi}{\partial \ln \theta} = c_p T, \tag{6}$$

which is an analogue of (1), Ψ' then decays upward. Higher, the cold anomaly in Figure 11 is replaced overhead and to its east by a warm anomaly, forming the mesospheric inversion. Coinciding with it in Figure 13 is strong positive vertical curvature of Ψ'.

[39] Figure 14 shows the contemporaneous map of Ψ at 61 km. The region of negative lapse rate (shaded) resembles the pattern of Ψ (contoured). In each, minimum values appear over Greenwich and extend westward along the Western Hemisphere, eventually crossing the dateline. The strongest negative lapse rate coincides with the minimum of Ψ. At higher levels, the inversion drives T' positive and therefore out of phase with Ψ', which is negative at these sites. Hydrostatic balance (6) then requires Ψ' to decay overhead. Planetary wave structure in Figure 13 decays above 60 km, notably, between Greenwich and the dateline, which in turn restores the vortex to polar symmetry.

[40] The correspondence to planetary wave activity and the impact exerted on the vortex by the mesospheric inversion are clearest in potential vorticity. It is plotted in Figure 15, along with horizontal motion, for the same time and level. At this mature stage of the warming, the vortex has been displaced out of polar symmetry and severely deformed by an intrusion of low-PV air that has invaded the polar cap. It induces an anticyclonic circulation at high latitudes, which draws high-PV air around it and westward. The head of the vortex (marked by maximum PV) is positioned over Greenwich. Extending from it is an elongated body that has been stretched along the Western Hemisphere and across the dateline. Mirroring the distorted structure of PV is the region of inverted thermal structure. Despite its severe distortion, contours of negative lapse rate remain virtually coincident with contours of high PV marking the vortex. In fact, at the rearward section of the vortex, PV contours break. Its tail then forms an isolated PV anomaly beyond the dateline. Collocated with it is an isolated anomaly of inverted thermal structure, which develops simultaneously.

[41] The mesospheric inversion brings about the decay of planetary wave structure in the upper mesosphere and lower thermosphere, where planetary waves experience strong absorption. In doing so, it acts to remove the PV anomaly disturbing the vortex, which is then restored toward polar symmetry at higher levels. Figure 16 shows the contemporaneous map of PV at 74 km. This level slices through the top of the inversion, where T' has shifted out of phase with Ψ', canceling planetary waves overhead. Strong distortion of the vortex, evident just 13 km below, has been almost eliminated. Although high PV and inverted thermal structure still evidence the crescent pattern, both have been largely restored to polar symmetry.

6. Conclusions

[42] Mesospheric inversions observed in vertical profiles by the lidar at OHP are part of a more extensive pattern that is closely related to planetary wave activity. The inversions form in association with an abrupt phase shift of planetary wave temperature. It drives wave temperature out of phase with wave geopotential, which in turn alters the vertical structure of planetary waves: from westward tilt and upward amplification below the inversion to nearly barotropic structure and decay above the inversion. Attending the upward decay of planetary waves is a relaxation of flow distortion, as the vortex is gradually restored towards polar symmetry.

[43] This behavior is favored during stratospheric warmings. Planetary waves are then amplified in the stratosphere and lower mesosphere, leading to a major displacement and distortion of the vortex. Both forms of zonal asymmetry decay in the upper mesosphere and lower thermosphere, as planetary waves experience strong absorption. The remarkable correspondence between inverted thermal structure and high PV marking the polar night vortex suggests a similar correspondence with other tracers. However, at the altitudes where mesospheric inversions form, chemical tracers become short lived, most having lifetimes far shorter than PV and the timescale of advection.

[44] The synoptic global structure considered here reveals a coherent pattern of inverted thermal structure, one that extends over large horizontal dimensions and is closely related to planetary wave structure. The correspondence between mesospheric inversions and planetary wave structure does not rule out contributions from other mechanisms. However, it makes clear that distortions of the circulation associated with planetary waves can produce inverted thermal structure that is coherent over large space scales and timescales. Even if the lapse rate is not fully reversed, the large-scale pattern of strengthened stability favors isolated inversions, which can be produced locally and intermittently by large-amplitude gravity waves and tides. In fact, individual UARS soundings include additional variability, which is noisier and operates coherently only on much shorter dimensions. Such variability may be a signature of gravity waves. By breaking and generating turbulence, they can participate, indirectly, in wave absorption, which alters the vertical structure of planetary waves above the layer of inverted thermal structure. Fully establishing the origin of mesospheric inversions will require a more comprehensive analysis that utilizes multiple lidar from around the globe, in concert with global thermal structure observed by satellite. It will also require a deeper understanding of dissipation mechanisms in the upper mesosphere and lower thermosphere, which limit upward propagation of planetary waves and render their structure barotropic.

References

Callaghan, P., A. Fusco, G. Francis, and M. Salby, A Hough spectral model for three-dimensional studies of the middle atmosphere, *J. Atmos. Sci.*, *56*, 1461–1480, 1999.

Francis, G., and M. Salby, Radiative influence of Antarctica on the polar night vortex, *J. Atmos. Sci.*, *58*, 1300–1309, 2001.

Fusco, A., and M. Salby, Interannual variations of total ozone and their relationship to variations of planetary wave activity, *J. Clim.*, *12*, 1619–1629, 1999a.

Fusco, A., and M. Salby, Interannual variations of total ozone and their relationship to variations of planetary wave activity: Corrigendum, *J. Clim.*, *12*, 3165, 1999b.

Hauchecorne, A., and M. L. Chanin, Density and temperature profiles obtained by lidar between 35 and 70 km, *Geophys. Res. Lett.*, *7*, 565–568, 1980.

Hauchecorne, A., M. L. Chanin, and R. Wilson, Mesospheric temperature inversion and gravity wave breaking, *Geophys. Res. Lett.*, *14*, 933–936, 1987.

Holton, J., *Introduction to Dynamic Meteorology*, 511 pp., Academic, San Diego, Calif., 1992.

Leblanc, T., and A. Hauchecorne, Recent observations of mesospheric temperature inversions, *J. Geophys. Res.*, *102*, 19,471–19,482, 1997.

Leblanc, T., A. Hauchecorne, M. L. Chanin, C. Rodgers, R. Taylor, and N. Livesey, Mesospheric temperature inversions as seen by ISAMS in December 1991, *Geophys. Res. Lett.*, *22*, 1485–1488, 1995.

Liu, H., M. Hagan, and R. Roble, Local mean state changes due to gravity wave modulated by the diurnal tide, *J. Geophys. Res.*, *105*, 12,381–12,396, 2000.

Salby, M., Climate monitoring from space: Asynoptic sampling considerations, *J. Clim.*, *2*, 1091–1105, 1989.

Salby, M. L., *Fundamentals of Atmospheric Physics, Int. Geophys. Ser.*, vol. 61, 628 pp., Academic, San Diego, Calif., 1996.

Sassi, F., and M. Salby, Fast Fourier synoptic mapping of UARS data, *J. Geophys. Res.*, *103*, 10,885–10,898, 1998.

Schmidlin, F., Temperature inversions near 75 km, *Geophys. Res. Lett.*, *3*, 173–176, 1976.

Wu, D., Mesospheric temperature inversion layers: Recent observations from UARS ISAMS and MLS, *Recent Res. Devel. Geophys.*, *3*, 37–44, 2000.

P. Callaghan and F. Sassi, Atmospheric Systems and Analysis, 1400 West 122nd Avenue Suite 101, Westminster, CO 80234, USA. (paddy@asac.org; sassi@thunder.asac.org)

A. Hauchecorne and P. Keckhut, Service d'Aeronomie, Centre National de la Recherche Scientifique, BP 3, Verrieres-le-Buisson, France. (alain.hauchecorne@aerov.jussieu.fr; philippe.keckhut@aerov.jussieu.fr)

M. Salby, Program in Atmospheric and Oceanic Sciences, University of Colorado, 311 UCB, Boulder, CO 80309, USA.

D. Wu, Jet Propulsion Laboratory, California Institute of Technology, 4800 Oak Grove Blvd., Pasadena, CA 91109, USA. (dwu@mls.jpl.nasa.gov)